

Seasonal and regional characterization of horizontal stirring in the global ocean

Ismael Hernández-Carrasco,¹ Cristóbal López,^{1*}
Emilio Hernández-García¹ and Antonio Turiel,²

¹Instituto de Física Interdisciplinar y Sistemas Complejos (CSIC-UIB)
07122 Palma de Mallorca, Spain

²Institut de Ciències del Mar, CSIC
Passeig Marítim de la Barceloneta 37-49, 08003 Barcelona, Spain

*To whom correspondence should be addressed; E-mail: clopez@ifisc.uib.es

Abstract

Recent work on Lagrangian descriptors has shown that Lyapunov Exponents can be applied to observed or simulated data to characterize the horizontal stirring and transport properties of the oceanic flow. However, a more detailed analysis of regional dependence and seasonal variability was still lacking. In this paper, we analyze the near-surface velocity field obtained from the *Ocean general circulation model For the Earth Simulator* (OFES) using Finite-Size Lyapunov Exponents (FSLE). We have characterized regional and seasonal variability. Our results show that horizontal stirring, as measured by FSLEs, is seasonally-varying, with maximum values in Summer time. FSLEs also strongly vary depending on the region: we have first characterized the stirring properties of Northern and Southern Hemispheres, then the main oceanic basins and currents. We have finally studied the relation between averages of FSLE and some Eulerian descriptors such as Eddy Kinetic Energy (EKE) and vorticity (ω) over the different regions.

1 Introduction

A detailed knowledge of the transport, dispersion, stirring and mixing mechanisms of water masses across the global ocean is of crucial interest to fully understand, for example, heat and tracer budgets, or the role of oceans in climate regulation. There has been a recent strong activity in the study of these processes from a Lagrangian perspective. Some works have addressed the *global* variability of them using finite-time Lyapunov exponents (FTLEs) computed from currents derived from satellite altimetry [4, 42]. These studies quantify stirring intensity, and identify mesoscale eddies and other Lagrangian Coherent Structures (LCSs). Furthermore, previous works [43] pointed out relationships between Lagrangian and Eulerian quantifiers of stirring/mixing activity (FTLEs and Eddy Kinetic Energy (EKE) or mean strain rate).

Having in mind the implications for the distribution of biogeochemical tracers, our goal is to extend the previous works to provide detailed seasonal analysis and a comparative study between different ocean regions and different scales: Earth's hemispheres, ocean basins, and boundary currents. To this end we use finite-size Lyapunov exponents

(FSLEs). These quantities are related to FTLEs since they also compute stretching and contraction time scales for transport, but they depend on explicit spatial scales which are simple to specify and to interpret in oceanographic contexts [10, 11, 20, 40]. In particular we will focus on the impact on transport of mesoscale processes, for which characteristic spatial scales as a function of latitude are well known. We are also interested in checking the existence of relationships between Lagrangian measures of horizontal stirring intensity, as given by averages of finite-size Lyapunov exponents (FSLE), and other dynamic, Eulerian quantities, such as EKE or vorticity. Such a functional relation does not need to hold in general, but may be present when there is a connection between the mechanisms giving rise to mesoscale turbulence (probably, baroclinic instability) and horizontal stirring.

The paper is organized as follows. In Section 2 we describe the data and tools used in this study. In section 3 we first present the geographical and seasonal characterization of the horizontal stirring, and then we investigate the relation of FSLE with EKE and vorticity. Finally, in the Conclusions we present a summary and concluding remarks.

2 Data and Methods

Our dataset consists of an output from the *Ocean general circulation model For the Earth Simulator* (OFES) [26, 25]. This is a near-global ocean model that has been spun up for 50 years under climatological forcing taken from monthly mean NCEP (United States National Centers for Environmental Prediction) atmospheric data. After that period the OFES is forced by the daily mean NCEP reanalysis for 48 years from 1950 to 1998. See [26] for additional details on the forcing. The output of the model corresponds to daily data for the last 8 years. Horizontal angular resolution is the same in both the zonal, ϕ , and meridional, θ , directions, with values of $\Delta\theta = \Delta\phi = 1/10^\circ$. The output has been

interpolated to 54 vertical z-layers and has a temporal resolution of one day. The velocity fields that we have used in this work correspond to the first two years, 1990 and 1991, of the output. Vertical displacements are unimportant during the time scales we consider here so that, despite horizontal layers are not true isopycnals, most fluid elements remain in their initial horizontal layer during the time of our Lagrangian computation. Thus we use in our analysis horizontal velocities in single horizontal layers. We refer to recent works [28, 6] for Lyapunov analyses considering vertical displacements. Unless explicitly stated, our calculations are for the second output layer, at 7.56 m depth, which is representative of the surface motion but limits the effect of direct wind drag (we have also studied the layer at 97 m depth; results on this layer are briefly shown in Fig. 3). See [26] and [25] for a thorough evaluation of the model performance.

Among Lagrangian techniques used to quantify ocean transport and mixing, local Lyapunov methods are being widely used. The idea in them is to look at the dispersion of a pair of particles as they are transported by the flow. To calculate FTLEs, pairs of particles infinitesimally close are released and their separation after a finite time is accounted; for FSLEs [2] two finite distances are fixed, and the time taken by pairs of particles to separate from the smallest to the largest is computed. Both methods thus measure how water parcels are stretched by the flow, and they also quantify pair dispersion. The methods can also be tailored to reveal two complementary pieces of information. On the one hand they provide time-scales for dispersion and stirring process [1, 2, 9, 23, 10, 19, 30]. On the other, they are useful to identify Lagrangian Coherent Structures (LCSs), persistent structures that organize the fluid transport [15, 13, 8, 21, 22, 24, 14, 37, 4, 11, 40, 29]. This second capability arises because the largest Lyapunov values tend to concentrate in space along characteristic lines which could often be identified with the manifolds (stable and unstable) of hyperbolic trajectories [15, 13, 14, 16, 37]. Since these manifolds are material

lines that can not be crossed by fluid elements, they strongly constrain and determine fluid motion, acting then as LCSs that organize ocean transport on the horizontal. Thus, eddies, fronts, avenues and barriers to transport, etc. can be conveniently located by computing spatial Lyapunov fields. We note however that more accurate characterization of LCSs can be done beyond Lyapunov methods [16], that high Lyapunov values can correspond also to non-hyperbolic structures with high shear [12], and that an important class of LCSs is associated to small, and not to large values of the Lyapunov exponents [35, 5].

In the present work, however, we are more interested in obtaining the first type of information, i.e. in extracting characteristic dispersion time-scales, quantifying the intensity of stirring, for the different ocean regions and seasons. In particular we want to focus on the transport process associated to eddies and other mesoscale structures. Previous Lagrangian analyses of the global ocean [4, 42] used FTLE to quantify such horizontal stirring. This quantity depends on the integration time during which the pair of particles is followed. FTLEs generally decrease as this integration time increases, approaching the asymptotic value of the infinite-time Lyapunov exponent [42]. We find difficult to specify finite values of this integration time for which easy-to-interpret results would be obtained across the different ocean regions. But for the mesoscale processes on which we want to focus, characteristic spatial scales are related to the Rossby Deformation Radius (RDR), with easily defined values and latitudinal dependence (see below). Thus, we use in this paper FSLEs as a convenient way to identify characteristics of stirring by mesoscale processes. FSLE are also convenient in finite ocean basins, where relevant spatial scales are also clearly imposed [1, 7, 23]. As a quantifier of horizontal stirring, measuring the stretching of water parcels, FSLEs give also information on the intensity of horizontal mixing between water masses, although a complete correspondence between stirring and

mixing requires the consideration of diffusivity and of the stretching directions [12].

More in detail, at a given point the FSLE (denoted by λ in the following) is obtained by computing the minimal time τ at which two fluid particles, one centered on the point of study and the other initially separated by a distance δ_0 , reach a final separation distance δ_f . At position \mathbf{x} and time t , the FSLE is given by: $\lambda(\mathbf{x}, t, \delta_0, \delta_f) = \tau^{-1} \ln(\delta_f/\delta_0)$. To estimate the minimal time τ we would need to integrate the trajectories of all the points around the analyzed one and select the trajectory which diverges the first. We can obtain a very good approximation of τ by just considering the four trajectories defined by the closest neighbors of the point in the regular grid of initial conditions at which we have computed the FSLE; the spacing of this grid is taken equal to δ_0 . The equations of motion that describe the horizontal evolution of particle trajectories are

$$\frac{d\phi}{dt} = \frac{u(\phi, \theta, t)}{R \cos \theta}, \quad (1)$$

$$\frac{d\theta}{dt} = \frac{v(\phi, \theta, t)}{R}, \quad (2)$$

where u and v stand for the zonal and meridional components of the surface velocity field coming from the OFES simulations; R is the radius of the Earth (6400 km), ϕ is longitude and θ latitude. Numerically we proceed by integrating Eqs. (1) and (2) using a standard, fourth-order Runge-Kutta scheme, with an integration time step $dt = 6$ hours. Since information is provided just in a discrete space-time grid, spatiotemporal interpolation of the velocity data is required, that is performed by bilinear interpolation. Initial conditions for which the prescribed final separation δ_f has not been reached after integrating all the available times in the data set are assigned a value $\lambda = 0$. A possible way to introduce small-scale features that are not resolved by our simulated velocity fields is by inclusion of noise terms in the equations of motion (2). We have recently shown [20]

that the main mesoscale features are maintained when this eddy-diffusivity is taken into account, though sub-mesoscale structures may change considerably. For global scales we expect the effects of noise to be even more negligible.

The field of FSLEs thus depends on the choice of two length scales: the initial separation δ_0 (which coincides with the lattice spacing of the FSLE grid and is fixed in our computations to the model resolution, $\delta_0=1/10^\circ$) and the final separation δ_f . As in previous works in middle latitudes [10, 11, 20] we will focus on transport processes arising from the mesoscale structures. In these studies δ_f was taken about $110km$, which is of the order of, but larger than, the mesoscale size in middle latitudes. Note that δ_f should be a decreasing function of the latitude, since mesoscale structures decrease in size with Rossby Deformation Radius (RDR). We need not to exactly match RDR but to guarantee that our choice of δ_f is similar but larger than mesoscale lengths, and also that it is a smooth function to avoid inducing artifacts. We have then chosen δ_f as $\delta_f = 1.3|\cos \theta|$ degrees; other reasonable choices lead to similar results to those presented here.

We compute the FSLEs by *backwards* time integration. In this way we quantify the fluid deformation by *past* stirring. When computing LCSs this leads to structures easier to interpret since they can be associated with the actual shape of tracer filaments [21, 11]. However, given that forward and backward exponents in incompressible flows are related by temporal shifts and spatial distortions [17], and that we are interested in temporal and spatial averages over relatively large scales, we do not expect significant differences when using *forward* exponents to calculate the stirring quantifiers presented below. This was explicitly checked in a similar framework in [10].

Lagrangian measurements have been shown to correlate well with several Eulerian quantities at several scales [43, 42]. In particular it is pertinent to correlate stirring with Eddy Kinetic Energy (EKE) since it is expected that more energetic turbulent areas

would also present stronger horizontal stirring, mainly due to the spawning of eddies (see however [34, 33]). Given an integration period T long enough (for instance $T =$ one year), the EKE (per unit of mass) is given by: $EKE = \frac{1}{2} \langle u'^2 + v'^2 \rangle$, where u' and v' are the instant deviations in zonal and meridional velocities from the average over the period T , and the brackets denote average over that period. Another Eulerian measurement used in this work is the surface relative vorticity, given by $\omega = \frac{\partial v}{\partial x} - \frac{\partial u}{\partial y}$, with positive (vs negative) ω associated to cyclonic (vs anticyclonic) motion in the Northern Hemisphere (opposite signs in the Southern Hemisphere). An additional Eulerian candidate to look for Lagrangian correspondences is the local strain rate, but it has been shown [43, 42] to scale linearly with $EKE^{1/2}$ and thus it will not be explicitly considered here.

Conditioned averages of λ as a function of another variable y (let y be $EKE^{1/2}$ or ω) introduced in Subsection 3.4 are obtained by discretizing the allowed values of y by binning; 100 bins were taken, each one defining a range of values (y_n, y_{n+1}) and represented by the average value $\hat{y}_n = \frac{y_n + y_{n+1}}{2}$. So, for each discretized value of \hat{y}_n the average of all the values of λ which occur coupled with a value in (y_n, y_{n+1}) is computed. The result is an estimate of the conditioned average $\tilde{\lambda}(y)$ (which is a function of y) at the points \hat{y}_n .

3 Results

3.1 Global horizontal stirring from FSLE

In Fig. 1 we present a map of FSLEs at a given time. Typical values are in the order of $0.1 - 0.6 \text{ days}^{-1}$, that correspond well to the horizontal stirring times expected at the mesoscale, in the range of days/weeks. Spatial structures, from filaments and mesoscale vortices to larger ones, are clearly identified; see a representative zoom of the South Atlantic Ocean (Bottom of Fig. 1), where the typical filamental structures originated by the horizontal motions are evident.

Instantaneous maps of FSLEs have a significant signature of short-lived fast processes and are adequate to extract LCSs, but we are more interested in slower processes at larger scales. We have hence taken time averages of FSLEs over different periods, in order to select the low-frequency, large-scale signal. In this way we can easily characterize regions in the global ocean with different horizontal stirring activity; areas with larger values of averaged FSLEs are identified as zones with more persistent horizontal stirring [10], as shown in Fig. 2a. As expected, we can observe that high stirring values correspond to Western Boundary Currents (WBCs) and to the Antarctic Circumpolar Current, while the rest of the ocean and the Eastern Boundary Currents (EBCs) display significantly lower values.

3.2 Geographical characterization of horizontal stirring

A convenient quantity used to characterize stirring in a prescribed geographical area A was introduced by [10], which is simply the spatial average of the FSLEs over that area at a given time, denoted by $\langle \lambda(\mathbf{x}, t) \rangle_A$. Time series of this quantity for the whole ocean and the Northern and Southern hemispheres are shown in Fig. 3a. It is worth noting that the stirring intensity is typically larger in the Northern Hemisphere than in the Southern one.

Further information can be obtained by analyzing the FSLE Probability Distribution Functions (PDFs). In Fig. 3b we present the PDFs for both hemispheres and the whole ocean; the required histograms are built using λ values computed once every week during one year (52 snapshots) at each point of the spatial FSLE grid in the area of interest. Each one of these PDFs is broad and asymmetric, with a small mode λ_m (i.e., the value of λ at which the probability attains its maximum) and a heavy tail. Similarly to what was discussed by [43] and [42] for the FTLE case, these PDFs are well described by Weibull

distributions with appropriate values for the defining parameters. We note that an explicit relationship between FTLE and FSLE distributions was derived by [41], but we have not checked if our flow is in the regime considered in that reference. The mode λ_m for the Southern Hemisphere is smaller than that of the Northern Hemisphere. Thus, Northern Hemisphere is globally more active in terms of horizontal dispersion than the Southern one. The same conclusions hold when looking at seasonally averaged instead of annually averaged quantities (not shown).

Taking into account the observed differences between Northern and Southern Hemispheres, we have repeated the same analyses over the main ocean basins in a search for isolating the factors which could contribute to one or another observed behaviors. In Fig. 3c we show the time evolution of $\langle \lambda \rangle_A$ as computed over the six main ocean basins (North Atlantic, South Atlantic, North Pacific, South Pacific, Indian Ocean and Southern Ocean), compared to the one obtained over the global ocean. The Southern Ocean happens to be the most active (in terms of horizontal stirring) because of the presence of the Antarctic Circumpolar Current, followed by the Atlantic and Indian Oceans, and finally the Pacific. We have also computed (Fig. 3d) PDFs of FSLE for the different oceans. As before, we obtain broad, asymmetric PDFs with small modes and heavy tails. The smallest mode λ_m corresponds to the Southern Pacific, meaning that there is less horizontal stirring activity in this basin, in support of what is also visually evident in Fig. 3c. On the opposite regime we observe that the largest FSLE values correspond to the Southern Ocean. For the rest of oceans the PDFs are rather coincident with the whole ocean PDF.

We have gone further to a smaller scale, by repeating the same analyses for the main currents in the global ocean: Gulf Stream, Benguela, Kuroshio, Mozambique, East Australian, California, Peru and Canary currents. As evidenced by Fig. 3e there is a clear separation in two groups of currents in terms of their horizontal stirring properties: the

most active currents (including Gulf Stream, Kuroshio, Mozambique and East Australian currents, all of them WBCs) and the least active ones (including Benguela, California, Peru and Canary Currents, which correspond to EBCs). The distinction remains in the PDF analysis: we can clearly distinguish two groups of PDFs: a) narrow PDFs highly peaked around a very small value of λ (EBCs); b) PDFs peaking at a slightly greater value of λ , but significantly broader (WBCs). Since the PDFs of the WBCs are broader, large values of FSLEs are found more frequently, i.e., more intense stirring occurs. This appears to be a reflection of the well-known mechanism of Western Intensification by [39]. Also, the asymmetry and tails of the PDFs show that the FSLE field is inhomogeneous and that there are regions with very different dispersion properties. Following [3], asymmetry and heavy tails make the PDFs quite different from the Gaussians expected under more homogeneous mixing. These characteristics are then indications that chaotic motion plays a dominant role versus turbulent, smaller scales, dynamics. That is, the large scale velocity features control the dynamics, something that is also reflected in the filamentary patterns of the LCS shown in Fig. 1.

3.3 Seasonal characterization of horizontal stirring

Horizontal stirring in the global ocean has a strong seasonal variability, as shown in Fig. 3a. Maximum values of $\langle \lambda \rangle_A$ in the Northern Hemisphere are reached early in that hemisphere Summer, and minimum ones early in that hemisphere Winter. The same happens for the Southern hemisphere related to its Summer and Winter periods.

Seasonally averaged FSLEs in the whole ocean over the four seasons are shown in Fig. 4. The spatial pattern is rather similar in all of them, and also similar to the annually-averaged spatial distribution shown in Fig 2a. Higher FSLE levels are found at the Gulf Stream and Kuroshio in the Northern Hemisphere in Spring and Summer of

that hemisphere. Analogously for the Eastern Australia and Mozambique Currents in the Southern Hemisphere relative to their own Spring and Summer time.

Following [44], to analyze which areas are more sensitive to seasonal changes, we computed the standard deviation of the annual time series of FSLE (see Fig. 5). Larger values appear to correspond to the more energetic regions thus showing a higher seasonal variability. More information about seasonal variability of different oceanic regions can be obtained again from Fig. 3. Time evolution of stirring in the North Atlantic and North Pacific, shown in Fig. 3c, attains high values in Spring and Summer, and minimum ones in Winter. Concerning the main currents, we found that values of stirring in Kuroshio, Gulf Stream, East Australia, and Mozambique currents increase in Spring and Summer and decrease in Winter (see Fig. 3e). This seasonal variability is also present in EBCs but the amplitude of the changes is smaller than in WBCs.

The generic increase in mesoscale stirring in Summer time detected here with Lyapunov methods has also been identified in previous works and several locations [18, 32, 27, 31, 44] (in most of the cases from the EKE behavior extracted from altimetric data). Although no consensus on a single mechanisms seems to exist (see discussion in [44]) enhanced baroclinic instability has been proposed in particular areas [32, 31], as well as reduced dissipation during Summer [44].

We have also calculated longitudinal (zonal) averages of the time averages of FSLE in Figs. 2a and 4. This is shown in Fig. 6 (top figure for the Northern hemisphere and bottom figure for the Southern one). First of all, we see that horizontal stirring has a general tendency to increase with latitude in both hemispheres. One may wonder if this is a simple consequence of the decreasing value of δ_f we take when increasing latitude. We have checked that the same increasing tendency remains when the calculation is redone with a constant δ_f over the whole globe (not shown), so that this trivial effect is properly

compensated by the factor $\ln(\delta_f/\delta_0)$ in the FSLE definition, and what we see in Fig. 6 is really a stronger stirring at higher latitudes. Note that this type of dependence is more similar to the *equivalent sea surface slope variability*, K_{sl} , calculated from altimetry in [38] than to the raw zonal dependency of the EKE obtained in the same paper. Since K_{sl} is intended to represent Sea Surface Height variability with the large scale components filtered out, we see again that our FSLE calculation is capturing properly the mesoscale components of ocean stirring observed by other means.

It is also clearly seen that latitudinal positions of local maxima of stirring correspond to the main currents (e.g. Gulf Stream and Kuroshio around 35°N; Mozambique, Brazil and East Australia around 25°S). The picture in Fig. 6 confirms that horizontal stirring is somehow higher in local Summer in mid-latitudes, where the main currents are, for both hemispheres. At low and high latitudes however the horizontal stirring is higher in local winter-time for both hemispheres, which is particularly visible in the Northern Hemisphere at high latitudes. A similar behavior was noted by [44] in the subpolar North Pacific and part of the subpolar North Atlantic for EKE derived from altimetry. Possible causes pointed there are barotropic instabilities or direct wind forcing.

3.4 Lagrangian-Eulerian relations

Lagrangian measures such as FSLEs provide information on the cumulative effect of flow at a given point, as it integrates the time-evolution of water parcels arriving to that point. They are not directly related to instantaneous measurements as those provided by Eulerian quantities such as EKE or vorticity, unless some kind of dynamic equilibrium or ergodicity-type property is established so that the time-integrated effect can be related to the instantaneous spatial pattern (for instance, if the spatial arrangement of eddies at a given time gives an idea about the typical time evolution of a water parcel) or

their averages. EKE gives information on the turbulent component of the flow, which is associated to high eddy activity, while relative vorticity ω takes into account the shear and the rotation of the whole flow. Eventual establishment of such dynamic equilibrium would allow to substitute in some instances time averages along trajectories by spatial averages, so providing a useful tool for rapid diagnostics of sea state. Thus, we will relate the Lagrangian stirring (as measured by the FSLEs) with an instantaneous, Eulerian, state variable. Of course, the Lagrangian-Eulerian relations will be useful only if the same, or only a few functional relationships hold in different ocean regions. If the relation should be recalculated for every study zone, the predictive power is completely lost.

We have thus explored the functional dependence of FLSEs with EKE and relative vorticity. In Fig. 2 the time average of these three fields is shown. Comparing FSLEs (Fig. 2a) and EKE (Fig. 2b), we see that high and low values of these two quantities are generally localized in the same regions. There are a few exceptions, such as the North Pacific Subtropical Countercurrent, which despite being energetic [32] does not seem to produce enough pair dispersion and stretching at the scales we are considering. It was already shown by [43] and [42] that variations in horizontal stirring are closely related to variations in mesoscale activity as measured by EKE. Note the similarity, with also an analogous range of values, of the EKE plot in Fig. 2b), obtained from a numerical model, to that of [42] (first figure), which is obtained from altimetry data. In [43] a proportionality between the stretching rate (as measured by FTLE) and $EKE^{1/4}$ was inferred for the Tasman Sea (a relation was found but no fit was attempted in the global data set described in [42]). In order to verify if a similar functional dependence between FSLE and EKE could hold for our global scale dataset, we have computed different conditioned averages (see Section 2), shown in Fig. 7: in the left panel we present the conditioned average $\tilde{\lambda}(EKE)$, while in the right panel $\tilde{\lambda}(\omega)$ is shown; both functions were

derived from the time averaged variables shown in Figure 2.

The smooth curve depicted in Fig. 7, left, is an indication of a well-defined functional relationship between $\bar{\lambda}$ and \overline{EKE} , similar to the ones found by [43] and [42] from altimeter data. Notice however that the plot just gives conditioned averages, but the conditioned standard deviation -which is a measure of randomness and fluctuations- is not negligible. An idea of the scatter is given for selected areas in Fig. 8. Considerably less compact relationships were obtained in the Mediterranean sea [11]. Fig. 8 shows that very different dynamical regimes identified by different values of λ may correspond to the same level of EKE. As a Lagrangian diagnostic, we believe that FSLE is more suitable to link turbulence properties to tracer dynamics than Eulerian quantifiers such as EKE. FSLEs provide complementary information since very energetic areas, with large typical velocities, do not necessarily correspond to high stretching regions. A paradigmatic example is a jet, or a shear flow, where small dispersions may be found because of the absence of chaotic trajectories. A functional relation between $\bar{\lambda}$ and $\bar{\omega}$ is also obtained (Fig. 7, right), although it is much noisier and probably worse-behaved. When particularizing for the different regions, we see that for EKE the WBCs are all roughly associated with one particular functional relation for the conditioned average $\bar{\lambda}$ while EBCs gather around a different one. None of the two prototype Lagrangian-Eulerian relations fits well to the relation $\lambda \propto EKE^{1/4}$ proposed for FTLE by [43] from altimeter data in the Tasman sea. Data are too scarce to make a reliable fitting for the conditioned average, in particular for the EBC. In Fig. 8 we see that relations of the form $\lambda \propto EKE^\alpha$ could be reasonably fitted to scatter plots of the data, with α larger than the 0.25 obtained in [43], specially for WBC where α is in the range (0.34, 0.40). This quantitative difference of our results with [43] may rest upon the fact that they considered just the Tasman Sea and we consider the different oceans. Other sources for the difference could be that we are using FSLE

of velocity data from a numerical model, instead of FTLE from altimetry, or that they use a grid of relatively low resolution $0.5^\circ \times 0.5^\circ$, while ours is $0.1^\circ \times 0.1^\circ$. Maybe their coarser resolution is not enough to resolve filaments which are the most relevant structures in our FSLE calculations. Despite this the qualitative shape of the Lagrangian-Eulerian relations is similar to the previous works [43, 42].

In order to analyze the ocean regions beyond boundary currents, we have also computed the conditioned averages for the Equatorial Current and for a 40° longitude by 20° latitude sub-region centered at 245° longitude and -30° latitude in the middle of the sub-tropical gyre in the Pacific Ocean (and hence an area of scarce horizontal stirring activity). We see (Fig. 7, left) that the EBC Lagrangian-Eulerian relation is valid for these two areas. We have also verified that the relations derived from annually-averaged quantities remain the same for seasonal averages (not shown). The important point here is the occurrence of just two different shapes for the EKE-FSLE relations across very different ocean regions, which may make useful this type of parametrization of a Lagrangian quantity in terms of an Eulerian one. For the relations of FSLE in terms of relative vorticity, a distinction between WBC and EBC still exists but the results are less clear and class separation is not as sharp as in the case of EKE (see Fig. 7, right). For instance, Gulf Stream and Kuroshio, despite being both WBC, do not seem to share the same Lagrangian-Eulerian relation, which limits its usefulness.

4 Conclusions

In this paper we have studied the space and time variability of horizontal stirring in the global ocean by means of FSLE analysis of the outputs of a numerical model. Similarly to what has been done in previous works, FSLEs can be taken as indicators of horizontal stirring. Being Lagrangian variables, they integrate the evolution of water parcels and

thus they are not completely local quantities. We have taken averages to analyze two main time scales (annual and seasonal) and three space scales (planetary scale, ocean scale and horizontal boundary scale). Our velocity data were obtained by using atmospheric forcing from NCEP. Structures and dynamics at small scales will be probably more realistic if forcing with higher resolution observed winds, as in [36]. But since we have not studied the first model layer which is directly driven by wind, and we have focused on averages at relatively large time and spatial scales, we do not expect much differences if using more detailed forcing.

Horizontal stirring intensity tends to increase with latitude, probably as a result of having higher planetary vorticity and stronger wind action at high latitudes, or rather, as argued in [44] because of barotropic instabilities. Certainly, new studies are required to evaluate these hypothesis. At a planetary scale we observe a significantly different behavior in the Northern hemisphere with respect to the Southern Hemisphere, the first being on average more active in terms of horizontal stirring than the second one. This difference can probably be explained by the greater relative areas of subtropical gyres in the Southern Hemisphere with small stirring activity inside them, which compensates in the averages the great activity of the Antarctic Circumpolar Current. At an ocean scale, we observe that the level of stirring activity tends to decay as the size of subtropical gyres increases, what is an indication that the most intense horizontal stirring takes place at the geographical boundaries of ocean basins. For that reason, we have finally analyzed the behavior of stirring at boundary scale, which is mainly related to WBCs and EBCs. EBCs behave in a similar way to ocean interior in terms of all the quantities we have computed, including the Lagrangian-Eulerian relations. Thus, the main hot spots of horizontal stirring in the ocean are WBC. The observed small mode in the global FSLE PDFs also indicates that horizontal stirring is not very intense for the vast majority of

the ocean, but the heavy tails indicate the existence of large excursions at some specific, stretched locations (e.g., inside the WBCs and other smaller scale currents active enough to generate stirring). This type of uneven distribution is characteristic of multifractal systems arising from large scale chaotic advection, something that was discussed for oceanic FSLEs in [20].

Regarding seasonal variability, generally we observe stronger stirring during each hemisphere's Summer time. Medium and high latitudes behave however in the opposite way: stirring is more active during the hemisphere Summer for medium latitudes and during the hemisphere Winter for high latitudes. Medium latitudes are strongly affected by the behavior of WBC, which experience intensification of horizontal stirring during Summer [18, 32, 27, 31, 44]. As commented before, high latitude Winter intense stirring could be the result of a stronger action of wind during that period or of barotropic instabilities [44], and dedicated studies are required to evaluate these hypothesis.

Finally, we have studied the connection between time-extended Lagrangian FSLEs and instant Eulerian quantities such as EKE and relative vorticity. For the case of EKE, the different ocean regions give rise to just two different Lagrangian-Eulerian relations, associated to an intense or a weak stirring regimes. The existence of these two regimes implies that pair dispersion and stretching strength are larger in a class of ocean areas (represented by WBC) than in another (e.g. EBC) at mesoscales, even when having the same EKE.

Acknowledgments

I.H.-C., C.L. and E.H.-G. acknowledge support from MICINN and FEDER through project FISICOS (FIS200760327); A. Turiel has received support from Interreg TOSCA project (G-MED09-425) and Spanish MICINN project MIDAS-6 (AYA2010-22062-C05-

01). The OFES simulation was conducted on the Earth Simulator under the support of JAMSTEC. We thank Earth Simulator Center-JAMSTEC team for providing these data.

References

- [1] V Artale, G Boffetta, A Celani, M Cencini, and A Vulpiani. Dispersion of passive tracers in closed basins: Beyond the diffusion coefficient. *Phys. Fluids*, 9:3162–3171, 1997.
- [2] E Aurell, G Boffetta, A Crisanti, G Paladin, and A Vulpiani. Predictability in the large: an extension of the Lyapunov exponent. *J. Phys. A*, 30:1–26, 1997.
- [3] F.J. Beron-Vera. Mixing by low- and high-resolution surface geostrophic currents. *J. Geophys. Res.*, 115:C10027, 2010.
- [4] F.J. Beron-Vera, M.J. Olascoaga, and G.J. Goni. Oceanic mesoscale eddies as revealed by Lagrangian coherent structures. *Geophys. Res. Lett.*, 35:L12603, 2008.
- [5] Francisco J Beron-Vera, Mara J Olascoaga, Michael G Brown, Huseyin Koak, and Irina I Rypina. Invariant-tori-like Lagrangian coherent structures in geophysical flows. *Chaos*, 20(1):017514, 2010.
- [6] J.H. Bettencourt, C. López, and E. Hernández-García. Oceanic three-dimensional Lagrangian coherent structures: A study of a mesoscale eddy in the Benguela upwelling region. *Ocean Modell.*, to appear, 2012.
- [7] G. Boffetta, A. Celani, M. Cencini, G. Lacorata, and A. Vulpiani. Non-asymptotic properties of transport and mixing. *Chaos*, 10:50–60, 2000.

- [8] G. Boffetta, G. Lacorata, G. Redaelli, and A. Vulpiani. Detecting barriers to transport: A review of different techniques. *Physica D*, 159:58–70, 2001.
- [9] G. Buffoni, P. Falco, A. Griffa, and E. Zambianchi. Dispersion processes and residence times in a semi-enclosed basin with recirculating gyres: An application to the Tyrrhenian sea. *J. Geophys. Res.-Oceans*, 102:18699–18713, 1997.
- [10] F. d’Ovidio, V. Fernández, E. Hernández-García, and C. López. Mixing structures in the Mediterranean sea from Finite-Size Lyapunov Exponents. *Geophys. Res. Lett.*, 31:L17203, 2004.
- [11] F. d’Ovidio, J. Isern-Fontanet, C. López, E. Hernández-García, and E. García-Ladona. Comparison between Eulerian diagnostics and Finite-Size Lyapunov Exponents computed from altimetry in the Algerian basin. *Deep-Sea Res. I*, 56:15–31, 2009.
- [12] Francesco d’Ovidio, Emily Shuckburgh, and Bernard Legras. Local mixing events in the upper-troposphere and lower-stratosphere. Part I: detection with the Lyapunov diffusivity. *J. Atmos. Sci.*, 66(12):3678–3694, 2009.
- [13] G. Haller. Distinguished material surfaces and coherent structure in three-dimensional fluid flows. *Physica D*, 149:248–277, 2001.
- [14] G. Haller. Lagrangian coherent structures from approximate velocity data. *Phys. Fluids*, 14:1851–1861, 2002.
- [15] G. Haller and G. Yuan. Lagrangian coherent structures and mixing in two-dimensional turbulence. *Physica D*, 147:352–370, 2000.

- [16] George Haller. A variational theory of hyperbolic Lagrangian coherent structures. *Physica D*, 240(7):574 – 598, 2011. Erratum and addendum: *Physica D* 241, 439–441 (2012).
- [17] George Haller and Themistoklis Sapsis. Lagrangian coherent structures and the smallest finite - time Lyapunov exponent. *Chaos*, 21(2):023115, 2011.
- [18] G Halliwell, D B Olson, and G Peng. Stability of the Sargasso Sea subtropical frontal zone. *J. Phys. Oceanogr.*, 24(6):1166–1183, 1994.
- [19] A. C. Haza, A. C. Poje, T. M. Özgökmen, and P. Martin. Relative dispersion from a high-resolution coastal model of the Adriatic Sea. *Ocean Modell.*, 22:48–65, 2008.
- [20] Ismael Hernández-Carrasco, Cristóbal López, Emilio Hernández-García, and Antonio Turiel. How reliable are finite-size Lyapunov exponents for the assessment of ocean dynamics? *Ocean Modelling*, 36(3-4):208 – 218, 2011.
- [21] B. Joseph and B. Legras. Relation between kinematic boundaries, stirring, and barriers for the Antarctic polar vortex. *J. Atm. Sci.*, 59:1198–1212, 2002.
- [22] T-Y. Koh and B. Legras. Hyperbolic lines and the stratospheric polar vortex. *Chaos*, 12(2):382–394, 2002.
- [23] G Lacorata, E Aurell, and A Vulpiani. Drifter dispersion in the Adriatic sea: Lagrangian data and chaotic model. *Ann. Geophysicae*, 19:121–129, 2001.
- [24] G. Lapeyre. Characterization of finite-time Lyapunov exponents and vectors in two-dimensional turbulence. *Chaos*, 12(3):688–698, 2002.

- [25] Yukio Masumoto. Sharing the results of a high-resolution ocean general circulation model under a multi-discipline framework - a review of OFES activities. *Ocean Dynamics*, 60:633–652, 2010.
- [26] Yukio Masumoto, Hideharu Sasaki, Takashi Kagimoto, Nobumasa Komori, Akio Ishida, Yoshikazu Sasai, Toru Miyama, Tatsuo Motoi, Humio Mitsudera, Keiko Takahashi, and et al. A fifty-year eddy-resolving simulation of the world ocean - Preliminary outcomes of OFES (OGCM for the Earth Simulator). *J. of the Earth Simulator*, 1(April):35–56, 2004.
- [27] Rosemary Morrow, Aurore Brut, and Alexis Chaigneau. Seasonal and interannual variations of the upper ocean energetics between tasmania and antarctica. *Deep-Sea Res. I*, 50(3):339–356, 2003.
- [28] T. M. Özgökmen, A. C. Poje, P. F. Fischer, and A. C. Haza. Large eddy simulations of mixed layer instabilities and sampling strategies. *Ocean Modell.*, 39:311–331, 2011.
- [29] Thomas Peacock and John Dabiri. Introduction to Focus Issue: Lagrangian coherent structures. *Chaos*, 20(1):017501, 2010.
- [30] Andrew C Poje, Angelique C Haza, Tamay M Özgökmen, Marcello G Magaldi, and Zulema D Garraffo. Resolution dependent relative dispersion statistics in a hierarchy of ocean models. *Ocean Modell.*, 31:36–50, 2010.
- [31] B Qiu and S Chen. Seasonal modulations in the eddy field of the South Pacific ocean. *J. Phys. Oceanogr.*, 34(7):1515–1527, 2004.
- [32] Bo Qiu. Seasonal eddy field modulation of the North Pacific Subtropical Countercurrent: TOPEX/Poseidon observations and theory. *J. Phys. Oceanogr.*, 29(10):2471–2486, 1999.

- [33] V. Rossi, C. López, E. Hernández-García, J. Sudre, , V. Garçon, and Y. Morel. Surface mixing and biological activity in the four Eastern Boundary upwelling systems. *Nonlin. Processes Geophys.*, 16:557–568, 2009.
- [34] V. Rossi, C. López, J. Sudre, E. Hernández-García, and V. Garçon. Comparative study of mixing and biological activity of the Benguela and Canary upwelling systems. *Geophys. Res. Lett.*, 35:L11602, 2008.
- [35] I I Rypina, F J Beron-Vera, M G Brown, H Kocak, M J Olascoaga, and I A Udovychenkov. On the Lagrangian dynamics of atmospheric zonal jets and the permeability of the stratospheric polar vortex. *J. Atm. Sci.*, 33149:3595, 2006.
- [36] Hideharu Sasaki, Yoshikazu Sasai, Masami Nonaka, Yukio Masumoto, and Shintaro Kawahara. An eddy-resolving simulation of the quasi-global ocean driven by satellite-observed wind field – preliminary outcomes from physical and biological fields -. *J. Earth Simulator*, 6:35–49, 2006.
- [37] Shawn C. Shadden, Francois Lekien, and Jerrold E. Marsden. Definition and properties of Lagrangian coherent structures from finite-time Lyapunov exponents in two-dimensional aperiodic flows. *Physica D*, 212(34):271 – 304, 2005.
- [38] Detlef Stammer. Global characteristics of ocean variability estimated from regional TOPEX/Poseidon altimeter measurements. *J. Phys. Oceanogr.*, 27(8):1743–1769, 1997.
- [39] H Stommel. The westward intensification of wind-driven ocean currents. *Trans. Amer. Geophys. Union*, 29(2):202–206, 1948.

- [40] E. Tew Kai, V. Rossi, J. Sudre, H. Weimerskirch, C. López, E. Hernández-García, F. Marsac, and V. Garçon. Top marine predators track Lagrangian coherent structures. *Proc. Natl. Acad. Sci. U.S.A.*, 106(20):8245–8250, 2009.
- [41] Alexandra Tzella and Peter H. Haynes. Smooth and filamental structures in chaotically advected chemical fields. *Phys. Rev. E*, 81:016322, Jan 2010.
- [42] D. W. Waugh and E. R. Abraham. Stirring in the global surface ocean. *Geophys. Res. Lett.*, 35:L20605, 2008.
- [43] D. W. Waugh, E. R. Abraham, and M. M. Bowen. Spatial variations of stirring in the surface ocean: A case of study of the Tasman sea. *J. Phys. Oceanogr.*, 36:526–542, 2006.
- [44] Xiaoming Zhai, Richard J. Greatbatch, and Jan-Dirk Kohlmann. On the seasonal variability of eddy kinetic energy in the Gulf Stream region. *Geophys. Res. Lett.*, 35:L24609, 2008.

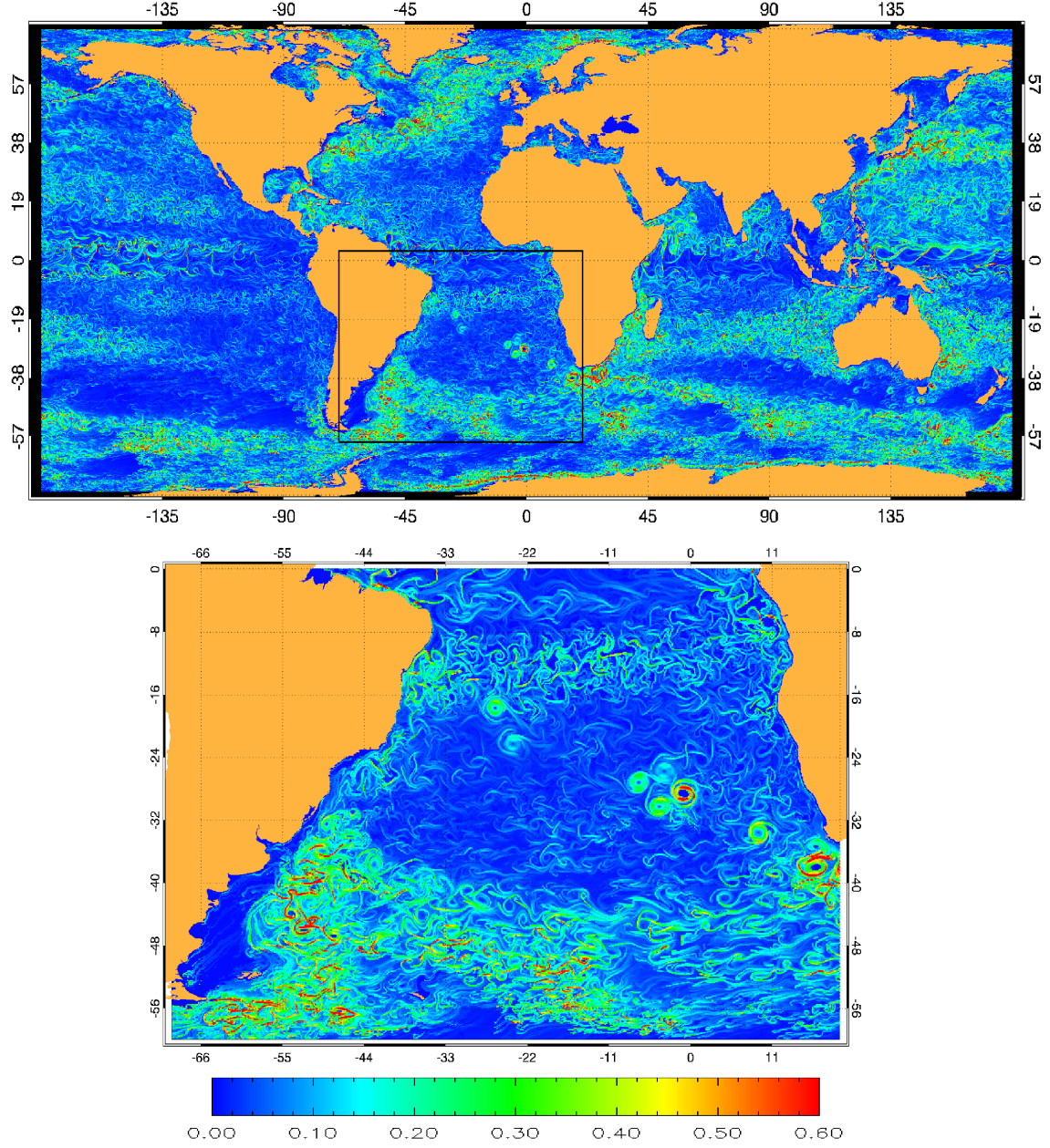


Figure 1: Top: Snapshot of spatial distributions of FSLEs backward in time corresponding to November 11, 1990 of the OFES output. Resolution is $\delta_0 = 1/10^\circ$. Bottom: Zoom in the area of the box inside top figure (South Atlantic Ocean). Coherent structures and vortices can be clearly seen. The colorbar has units of day^{-1} .

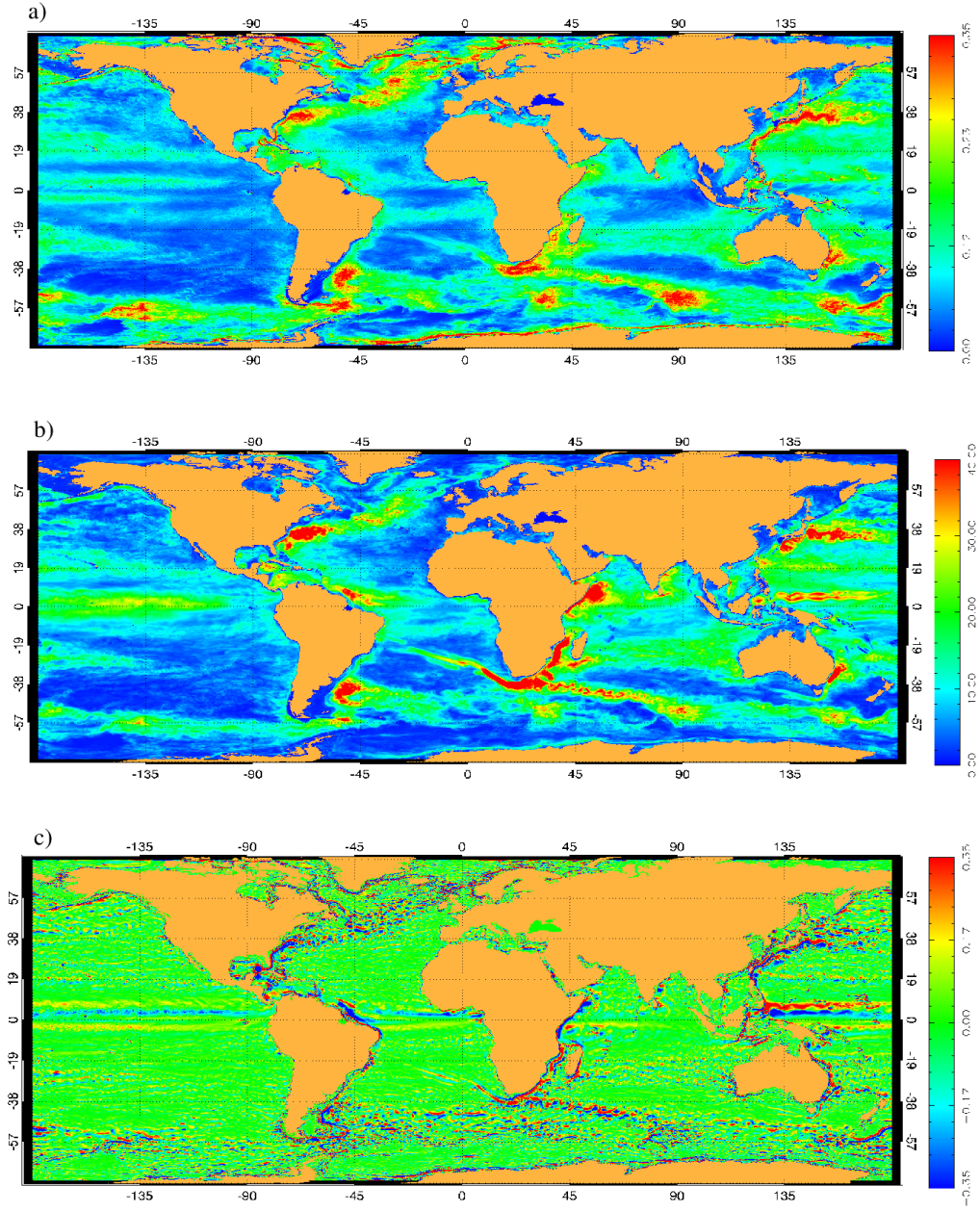


Figure 2: a) Time average of the FSLEs in the Global Ocean. Geographical regions of different stirring activity appear. The colorbar has units of day^{-1} . b) Spatial distribution of annual $EKE^{1/2}$ (cm/s). c) Time average of Relative Vorticity (ω) in the Global Ocean. The color bar has units of day^{-1} . In all the plots the averages are over the 52 weekly maps computed from November 1st, 1990 to October 31th, 1991.

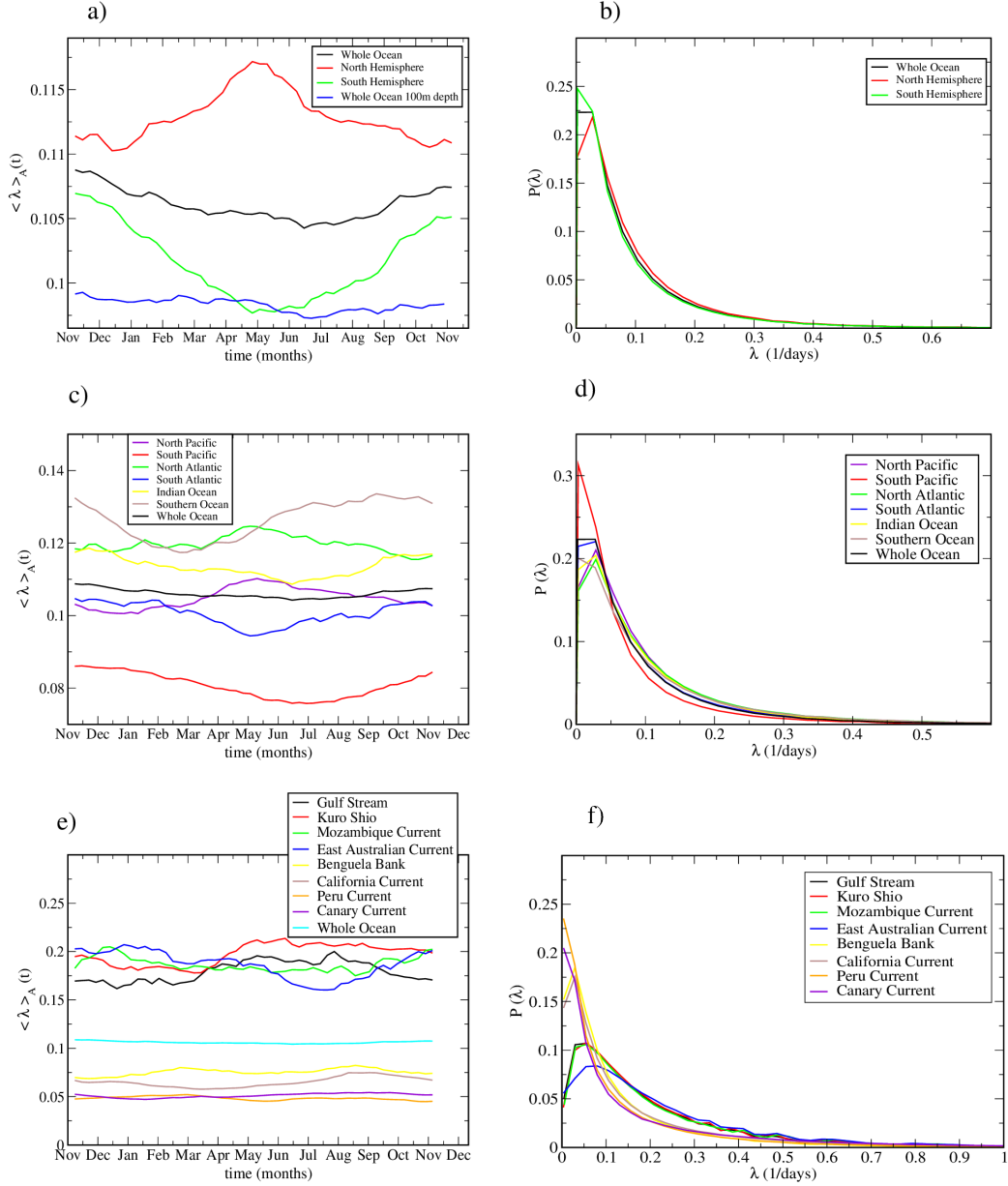


Figure 3: Left column: Temporal evolution (from November 1st, 1990 to October 31th, 1991) of the horizontal stirring (Spatial average of FSLEs). Right column: PDFs of the FSLEs (histograms are built from the λ values contained at all locations of the 52 weekly maps computed for the second simulation output year). Top: for both hemispheres and for the whole ocean. Middle: for different oceanic regions. Bottom: for some main currents during one simulation year. In addition to the results from the second surface layer analyzed through the paper, panel a) shows also stirring intensity in a layer close to 100m depth.

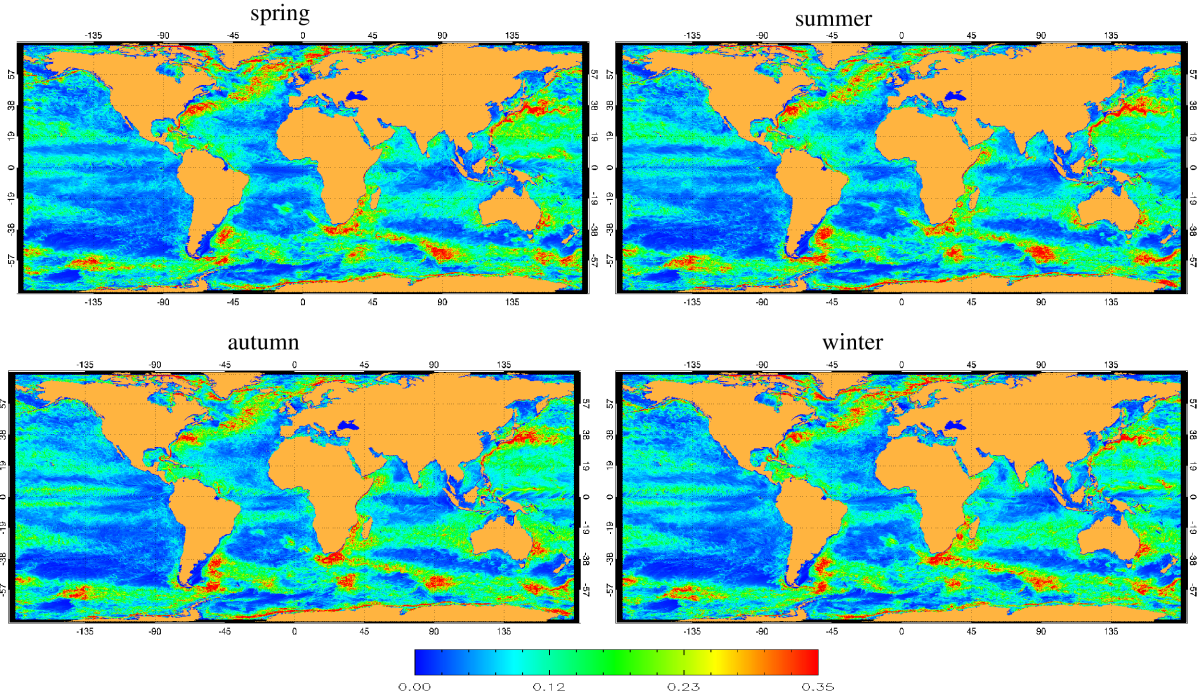


Figure 4: Time average of the FSLEs in the Global Ocean for the each season. Spring: from March 22 to June 22. Summer: from June 22 to September 22. Autumn: from September 22 to December 22. Winter: from December 22 to March 22. The colorbar has units of day^{-1} .

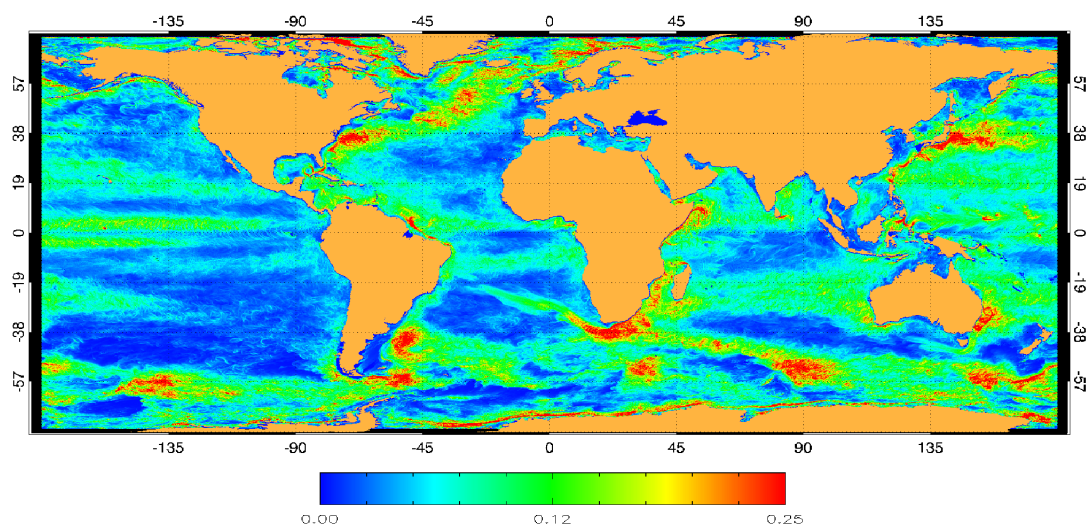


Figure 5: Standard deviation of weekly FSLE maps of one year. The colorbar has units of day^{-1}

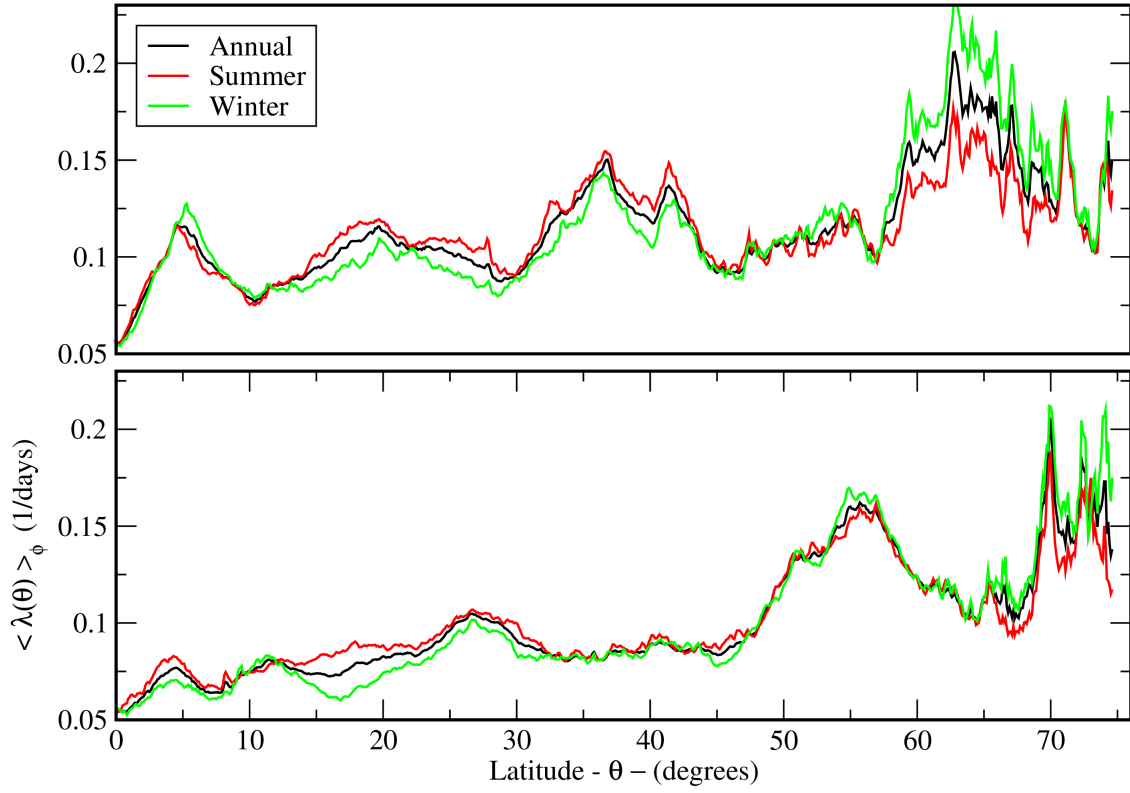


Figure 6: Cross-ocean zonal average of the annual, relative Summer and relative Winter time average of FSLE maps from Fig 2a as a function of latitude (expressed as absolute degrees from Equator to make both hemispheres comparable). Top: Northern Hemisphere; bottom: Southern Hemisphere.

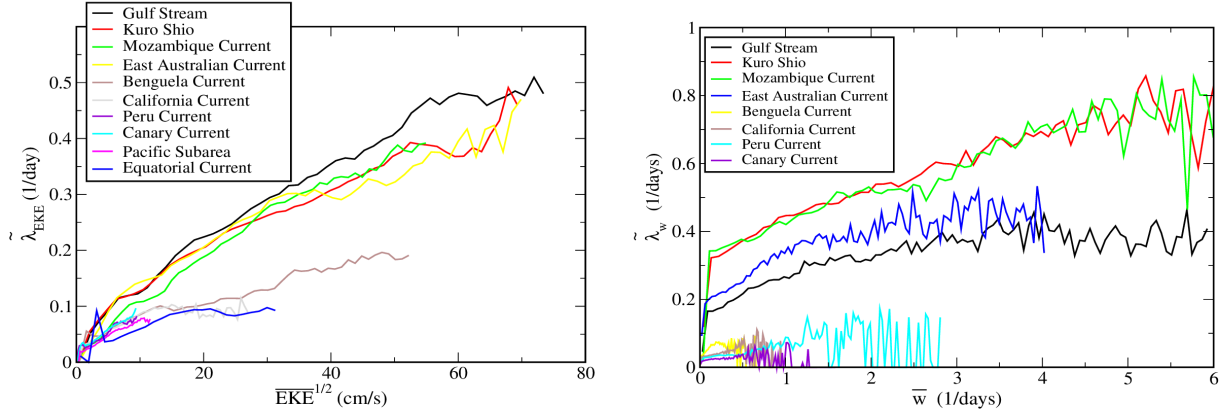


Figure 7: Left: Lagrangian-Eulerian relations. Left: the conditional average $\tilde{\lambda}_{EKE}$ as a function of its corresponding annually averaged (second year) \overline{EKE} for different regions and currents. We clearly observe two groups of relations FSLE-EKE. Right: same plot for the conditional average $\tilde{\lambda}_{\omega}$ as a function of its corresponding annually averaged (second year) $\overline{\omega}$. Although we observe also the same two two groups of FSLE- ω relations, these functions are much noisier and region-dependent.

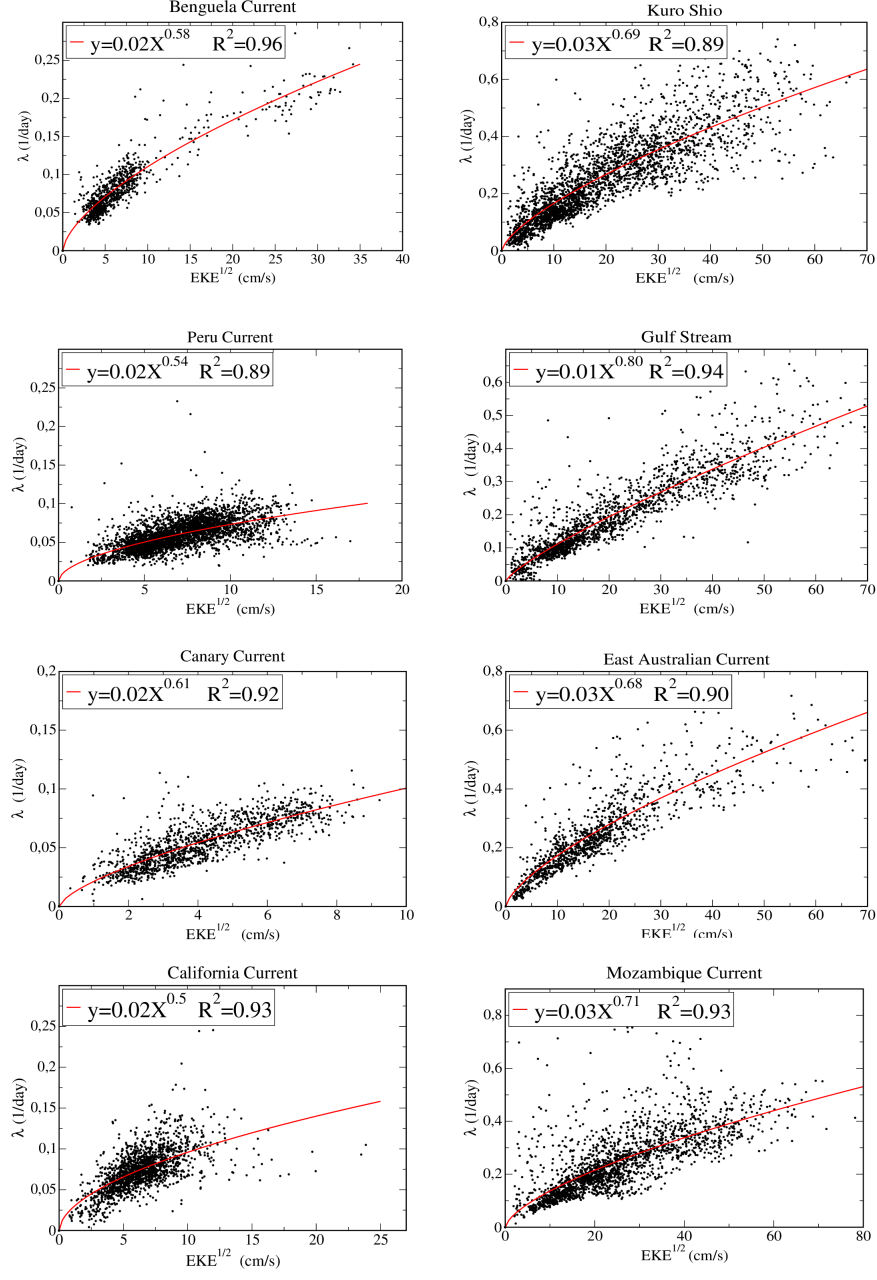


Figure 8: Scatter plots showing temporally averaged FSLE values at different spatial points in regions of Fig. 2a, and EKE values (as displayed in Fig. 2b) at the same points. The regions displayed here are eight of the main currents. Fittings of the type $y = cX^b$ are also displayed, where y is the temporal mean of FSLE and X is $EKE^{1/2}$. Note that this implies $\langle \text{FSLE} \rangle = c EKE^\alpha$ with $\alpha = b/2$.